Scanning-helium-ion-beam lithography with hydrogen silsesquioxane resist

D. Winston[a)] and B. M. Cord
Massachusetts Institute of Technology, Cambridge, Massachusetts 02139

B. Ming
National Institute of Standards and Technology, Gaithersburg, Maryland 20899

D. C. Bell
Harvard University, Cambridge, Massachusetts 02138

W. F. DiNatale and L. A. Stern
Carl Zeiss SMT Inc., Peabody, Massachusetts 01960

A. E. Vladar and M. T. Postek
National Institute of Standards and Technology, Gaithersburg, Maryland 20899

M. K. Mondol, J. K. W. Yang, and K. K. Berggren
Massachusetts Institute of Technology, Cambridge, Massachusetts 02139

A scanning-helium-ion-beam microscope is now commercially available. This microscope can be used to perform lithography similar to, but of potentially higher resolution than, scanning electron-beam lithography. This article describes the control of this microscope for lithography via beam steering/blanking electronics and evaluates the high-resolution performance of scanning helium-ion-beam lithography. The authors found that sub-10 nm-half-pitch patterning is feasible. They also measured a point-spread function that indicates a reduction in the micrometer-range proximity effect typical in electron-beam lithography. © *2009 American Vacuum Society.*
[DOI: 10.1116/1.3250204]

I. INTRODUCTION

Focused ion beam (FIB) technology can be used for patterning of materials down to ≈ 10 nm but not far below that. A common use of FIB is direct subtractive patterning of a substrate, the so-called ion milling, which can achieve feature sizes of ≈ 10 nm in some cases.[1] A less common use of FIB is for conventional lithography, i.e., patterning of sacrificial thin films ("resists," named so for their etch resistance) for subsequent pattern transfer.[2] As early as 18 years ago, sub-10 nm wide lines were fabricated in poly(methyl-methacrylate) (PMMA), a common electron-beam resist, using a Ga^+ FIB.[3] However, half-pitch has not yet reached 10 nm using FIB lithography. Barriers to such a half-pitch include system optics and the interaction of the ion species with the resist and underlying substrate (see Fig. 1). In this article, we have used a high-brightness He^+ FIB system with a high-contrast resist process to lower these barriers, achieving 10 nm half-pitch with good feature separation, and 5 nm half-pitch with poor but resolvable separation.

In lithography a finite point-spread function (PSF) results in the exposure of unwanted features between closely spaced intended features; the overlapping exposure dose tails of neighboring features add and may sum up to an appreciable dose. Figure 1 shows that spot size, forward- and back-scattering range ("straggle" being the standard deviation of the spatial distribution), and secondary electron range determine the PSF that limits resolution. Ramachandra *et al.* pro-

vide a useful introduction to and discussion of these and other contributing factors to resolution with electron and helium-ion beams.[4]

One may expect the achievable spot size of a focused helium-ion beam to be smaller than that of an electron beam. The specified spot size for a Zeiss Orion Plus helium-ion microscope is ≤ 0.75 nm at an accelerating voltage of ≈ 30 kV. The spot size is limited by spherical/chromatic aberration. Aberrations are reduced by using smaller beam-limiting apertures, thus reducing the focusing angle through column components. Helium ions are more massive than electrons by over three orders of magnitude and thus diffract less around apertures. Thus, smaller apertures are possible in a helium-ion column than in an electron column, and this enables a smaller spot size. However, a smaller aperture means lower beam current, which makes focusing difficult. The small virtual source size and high brightness of the Orion system, which will be discussed later, are innovations that enable sufficient current to realize sub-1 nm spot size.

Prior work indicates that lower-energy secondary electrons (SEs) are generated by ion beams relative to electron beams of the same incident kinetic energy.[5] In an elastic binary collision between a 30 keV He^+ and a stationary electron, the He^+ will transfer a maximum energy of ≈ 16 eV to the electron (in contrast, a 30 keV electron can theoretically transfer all of its energy to a stationary electron in such a collision). To relate this energy transfer to resist patterning, consider hydrogen silsesquioxane (HSQ), a negative-tone electron-beam resist that cross-links via Si–H bond scission.[6] The energy of a Si–H bond is ≈ 3 eV, so secondary electrons

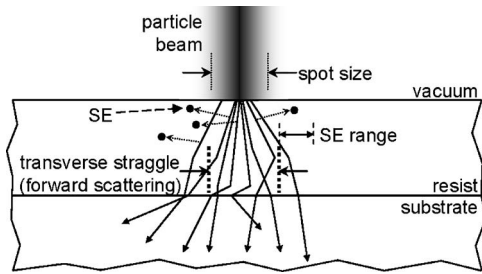---

[a)]Electronic mail: dwinston@mit.edu

FIG. 1. Three major factors that limit resolution are illustrated: (1) spot size at the vacuum-resist interface sets a lower bound on resolution, (2) scattering, and (3) secondary electron (SE) generation create an interaction volume in the resist greater than the product of projected range (depth of implantation) and spot cross section; transverse straggle is the standard deviation of the lateral particle distribution in the resist due to scattering. This figure ignores backscattering (the scattering of incident particles back to the vacuum-resist interface) for simplicity of illustration, but such scattering could adversely affect resolution.

may break bonds and thus help cross-link HSQ. In this way, secondary electrons may broaden the PSF. It is unclear whether lower-energy SEs from helium-ion exposure result in a reduced SE range and thus a correspondingly narrower PSF than with electron exposure at similar incident energies; recent simulation of a measure of SE range found similar values for both electron-induced SEs and helium-ion-induced SEs.[4]

Helium ions scatter less than electrons, without inducing recoil-atom scattering to the extent that heavier ions do. The transverse (lateral) straggle of a focused helium-ion beam will be smaller than that of a focused electron beam because helium ions are more massive than electrons, and thus helium ions undergo less elastic scattering. "Heavy" ions such as Ga^+ may displace and scatter atoms in the substrate so much that device performance suffers.[5] He^+ may cause such damage as well, but only at a fluence above 5×10^{15} ions/cm^2,[7] and such a high fluence is not needed for He^+ lithography.[8] Because helium ions scatter less than electrons, without inducing recoil-atom scattering to the extent that heavier ions do, the helium-ion PSF should be correspondingly narrower than electron or heavy-ion PSFs.

Prior work on ion lithography has included projection through a stencil mask,[9] proximity printing through a stencil mask,[5,10] scanning a focused beam for gas-assisted deposition,[11] and scanning a focused beam for resist patterning. Because scanning-beam resist patterning requires neither an intermediate lithographic product, i.e., a mask, nor injection of precursor gasses and is thus quite flexible for writing arbitrary patterns, we used scanning-beam, resist-based lithography in order to test resolution. Past work in this area has included a variety of ion species and a variety of resists. Horiuchi *et al.* achieved 200 nm linewidth in PMMA using a He^+ beam.[12] Van Kan *et al.* demonstrated 22 nm linewidth in HSQ using a 2 MeV H_2^+ beam.[13] Kubena *et al.* achieved sub-20 nm linewidth in PMMA using a Ga^+ beam;[14] the same set of authors later improved this to linewidths as small as 8 nm with 100 nm pitch,[3] and predicted in this latter article that higher-resolution results may be possible with a

higher-contrast, lower-sensitivity (to reduce statistical dose fluctuations) resist process and with a source of ions lighter than Ga^+ (such as He^+). We agree that these elements may be what were lacking in the pursuit of higher-resolution scanning-ion-beam lithography.

II. EXPERIMENTAL APPROACH

High-resolution resist patterning with a helium-ion beam requires an ion source with adequate brightness and apparatus for accurate beam positioning and modulation, a resist and development process with sufficient resolution, and metrological methods capable of assessing the resultant sub-10 nm features. But these elements were unavailable until recently: helium-ion sources were too dim to be of great use in lithography; and resists with robust sub-10 nm resolution were difficult to image and measure. To resolve these problems, we used a recently developed helium-ion microscope (Orion Plus, Carl Zeiss SMT)[15] with a commercial pattern generator (NPGS 9.0, Nabity); HSQ resist[6] with a new high-contrast development process;[16] and conventional field-emission scanning-electron microscopes (FE-SEMs) capable of yielding high-resolution, high-contrast images of the patterned HSQ directly, without requiring pattern transfer to another material. We will now describe each of these system elements in turn.

The helium-ion-microscope parameters that place limits on our lithographic performance include source brightness, energy spread, beam current, and system stability during exposure. The source brightness has been documented as 4×10^9 A cm^{-2} sr^{-1} (or 250 ions μs^{-1} nm^{-2} μsr^{-1}); the energy spread has been measured as 1 eV or smaller; and the virtual-source diameter has been estimated as 0.3 nm.[15] A beam current of $0.5-1$ pA is specified for smallest spot size (≤ 0.75 nm), but any current between 1 fA and 100 pA should be usable. The gun tip is structured as an inverted pyramid of W atoms that terminates at its apex with a set of three atoms; when gun temperature exceeds 95 K, this structure is unstable, meaning source size and thus brightness may become compromised at higher temperatures.[15] However, gun cooling causes vibration in our system, so active cooling is normally turned off during high-resolution image acquisition, and so we turned off active cooling during pattern exposure. Considering adverse effects of gun heating, such as aperture misalignment and a decrease in beam current, we limited experimental writing sessions to less than 5 min at a time. We did not directly measure current stability and beam shape over time.

Although the helium-ion-beam microscope can exhibit a small beam size, only relatively simple dot-array patterns can be formed using the native raster-scan generator of this system. To form more complex patterns, we used a commercial pattern generator. The Nabity NPGS consisted of PCI-card hardware with output connectors for beam blanking and steering, CAD software for pattern layout, and control software for pattern writing. The system was capable of 16-bit stepping (65 536 positions) across each scan dimension and a

maximum step frequency of 5 MHz. The only additional hardware necessary was a passive adapter cable that we constructed.

In order to extend the resolution of ion-beam lithography, a resist process was required with two key capabilities: sub-10 nm resolution and ease of developed-pattern inspection in readily available metrology tools. We used HSQ resist[6] and salty development,[16] which has achieved 7 nm half-pitch in published work;[16] 4.5 nm half-pitch has recently been demonstrated using this material by a team at MIT and Raith USA that included some of the authors of this article.[17] Because exposed HSQ is like silica and thus has high SE yield, unlike a carbon-based resist such as, e.g., poly(methyl methacrylate), even sub-10 nm length-scale HSQ patterns on silicon are resolvable with good contrast in a scanning-electron microscope (SEM) without requiring additional processing.

To evaluate the patterning resolution of our system, we used small-pitch nested-"L" structures. Nested-L's are convenient test structures for high-resolution lithography because (1) they test corner sharpness and the PSF narrowness via the L joints, (2) they test beam stigmation via orthogonal grating exposures, and (3) they further test the PSF narrowness by including both isolated and dense features. Such structures cannot be fabricated with a scanning-beam microscope without a pattern generator. Nested-L lines were defined to be one pixel wide, and nested-L structures had pitches of 10, 20, 30, 40, and 50 nm.

To determine the lithographic PSF of the focused helium-ion beam, we exposed single dots at various doses (an explicit description of such a method may be found in Ref. 18). Single-dot exposures, assuming a high-contrast resist, could provide valuable information about the spatial dose distribution of a focused helium-ion-beam "spot." We exposed an array of dots at each dose. Dot arrays were 1×1 or 2×3 μm^2 rectangular arrays of single-pixel exposures, with pitches of 50, 100, 200, 250, and 500 nm. Instead of specifying a dot array as a collection of dot objects, we defined a rectangle object and specified dot pitch as the beam step size for a raster-scanned "filling in" of the rectangle; specifying a collection of dot objects would have lengthened the total exposure time because of necessary beam-settling time before exposing each CAD-file object.

Two samples were processed successfully. The first of these had good dot-exposure data but did not yield nested-L structures due to insufficient dose. The second had good results for both dots and nested-L's. We designate these samples as samples A and B, respectively, and we will now describe their preparation, exposure, development, and metrology.

Preparation was similar for both samples. For sample A, we spin coated 2% HSQ in methyl isobutyl ketone (XR-1541, Dow Corning) onto an ~ 1 cm^2 cleaved chip of a prime silicon wafer at 6 krpm for 1 min using the minimum startup acceleration of our spinner (unmeasured). Adhesion of resist was deemed adequate by visual inspection. We did no pre-exposure baking of the sample. Resist thickness was measured to be 31 nm using a single-angle, single-wavelength ($\lambda = 632.8$ nm) ellipsometer that assumed a HSQ index of refraction of $n = 1.41$ (specified by the manufacturer). Then, a diamond-tipped scribe was used to scratch the sample to provide an artifact for focusing and stigmation near the exposure area. The preparation of sample B was identical to that of sample A, with the exception that sample B used the maximum startup acceleration (but also to 6 krpm) of our spinner. This difference is not expected to be of technical significance. The measured thickness of sample B was 25 nm.

Exposure conditions were similar for both samples, so parameters for which differences are not expected to be of technical significance will be listed as the average (with reduced precision) for both samples. Helium pressure, which was modulated to extract sufficient current from the gun, was 3×10^{-4} Pa (2×10^{-6} Torr); acceleration voltage, which was fixed by the structure of the gun and changes each time the gun tip is rebuilt, was 27 kV; beam-limiting-aperture diameter was 10 μm (equal for both samples); beam current was 0.2 pA; working distance from the final lens to the sample was 7 mm; and total exposure time was 2 min. One difference of potential significance was that for sample A, gun temperature ramped from 88 to 90 K, whereas for sample B, gun temperature ramped from 78 to 80 K. The dose series for the samples spanned different but overlapping ranges. For sample A, point doses for eight dot-array structures ranged from 0.018 fC (100 μs per dot) to 0.36 fC (2 ms per dot) in a geometric progression. For sample B, point doses for ten dot-array structures ranged from 0.15 fC (536 μs per dot) to 15 fC (53.571 ms per dot) in a geometric progression. For sample B's nested-L structures, ten line doses ranged from 0.05 nC/cm (22.4 μs per 1.25 nm step) to 0.5 nC/cm (223.3 μs per step) in a geometric progression. Note that an isolated dot (actually a pillar because resist thickness was larger than beam size) requires more dose than a step along a line because the dose distributions of adjacent line-step exposures overlap.

Samples A and B were developed in the same manner. We used a salty, alkaline solution previously shown to increase the contrast of electron-irradiated HSQ.[16] The developer was prepared by dissolving 10 g NaOH pellets and then 40 g NaCl crystals in 1 l de-ionized water, resulting in a 1% NaOH, 4% NaCl solution (w/v). The sample was immersed in ≈ 40 ml of this solution for 4 min at room temperature (unmeasured), rinsed in de-ionized water for 1 min, and blown dry with a N_2 gun.

For metrology, both samples were imaged in FE-SEMs. Sample A was cleaved after development to fit onto the sample chuck for a Hitachi S-5500 cold-FE SEM. The small sample chuck enabled special "in-lens" sample positioning—the sample was placed within part of the final objective lens, which resulted in very small working distances: we took secondary electron images at a working distance of 0.6 mm and an accelerating voltage of 5 kV. Sample B was imaged with the in-lens secondary electron detector of a Zeiss Leo 1500-series Schottky thermal-FE SEM (part of a Raith 150
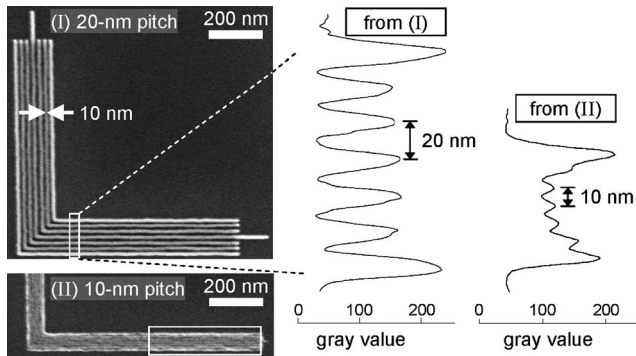
FIG. 2. (I) Scanning-electron micrograph of helium-ion-patterned, 20 nm pitch nested Ls of 25-nm-thick HSQ on silicon; line dose was 0.232 nC/cm (exposure step size was 1.25 nm and dwell time per exposure point was 104 μs). (II) A region of 10 nm pitch nested Ls at the same imaging magnification as (I); the line dose was 0.0834 nC/cm or $\approx$50 ions/nm (exposure step size was 1.25 nm and dwell time per exposure point was 37.3 μs). Averaging across each row of pixel values in the white-boxed areas obtained cross-sectional slices that show the modulation apparent in each nested-L structure. Both structures are from sample "B" (see text for processing details).
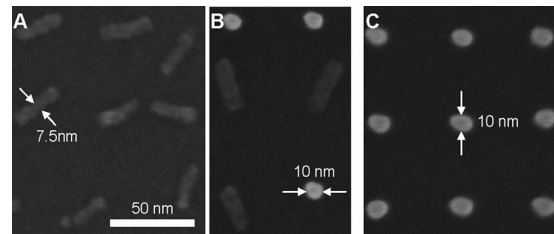

FIG. 3. Variation in pillar diameter and observation of pillar collapse with varying dose of point exposures in 31-nm-thick HSQ on silicon. (a) 0.21 fC/pillar ($\approx$1300 ions); (b) 0.31 fC/pillar ($\approx$1900 ions); (c) 0.36 fC/pillar ($\approx$2200 ions). All scanning-electron micrographs have the same magnification. Pillar collapse at lower doses may have been due to the large aspect ratio (up to $\approx$4:1) and resulting mechanical instability during solvent development. All structures depicted are from sample "A" (see text for processing details). Each dot array spanned a 2×3 μm^2 "block," with varying point dose from block to block. Since the dots were not considered separate structures by the pattern-generation software, there was no settling time before each dot exposure; this reduced total exposure time, but may have negatively impacted placement accuracy.

electron-beam lithography system); accelerating voltage was 5 kV, beam-limiting-aperture diameter was 30 μm, and working distance was 3 mm.

III. RESULTS AND ANALYSIS

We were able to fabricate 20 nm pitch HSQ structures with little resist residue between developed features and 10 nm pitch structures with considerable residue. Figure 2 shows images of 20 nm pitch and 10 nm pitch nested L's, both at the same imaging magnification; to clarify modulation in the secondary electron images at each of the two pitch values, we also show pixel-averaged slices through a grating region within each image.

The line dose to yield single-pixel lines appears to lie between 0.083 nC/cm ($\approx$50 ions/nm) and 0.23 nC/cm ($\approx$140 ions/nm) (above 0.23 nC/cm, we saw no collapse/ uprooting of $\approx$3:1 height:width lines), an order of magnitude lower than the dose to print for HSQ on silicon using electron-beam lithography.[19] Such a difference in dose to print is a consequence of the increased stopping power, i.e., energy deposited per unit length of travel in a material, of an incident ion relative to that of an incident electron of similar energy.

Figure 3 depicts some of our fabricated dot-array structures. Because the resist was thicker than the beam size, pillar structures formed. At low doses the pillar aspect ratio was $\approx$4:1, and this made the pillars more susceptible to collapse, possibly via capillary forces during the drying process after development. The point-dose-to-yield for dot features appears to lie between 0.15 fC ($\approx$1000 ions) and 0.35 fC. Beyond $\approx$0.35 fC/pillar ($\approx$2200 ions), we observed no pillar collapse.

We have estimated the lithographic PSF for our focused helium-ion beam in HSQ on silicon. From SEM images of 50 nm pitch dot arrays at each of 15 doses, we selected ten pillars at random and measured their widths (we noticed no

relationship between dot-array pitch and dot width at any dose). Figure 4 is a semilog plot of dose density, which is proportional to the reciprocal of beam dwell time, versus half the measured pillar diameter. A double-Gaussian function appears to fit the data well. A double Gaussian is often presumed for the PSF of an electron beam, for which the smaller-spread Gaussian (typically $\alpha \approx 10-50$ nm) represents the effect of forward scattering, and the larger-spread, smaller-amplitude Gaussian (typically $\beta \approx 1-10$ μm) represents the effect of backscattering. The model parameters we obtained ($\alpha \approx 4$ nm, $\beta \approx 14$ nm) indicate that forward scattering was perhaps slightly reduced relative to an electron beam and that long-range backscattering, at least for the dose range tested, was absent (it is not clear what the β term represents physically in our case). We expect little long-range backscattering due to the difference in behavior of electrons and helium ions in a solid.

$$\mathrm{PSF}(r) = A\left[\frac{1}{\alpha^2}\exp\left(-\left(\frac{r}{\alpha}\right)^2\right) + \frac{\eta}{\beta^2}\exp\left(-\left(\frac{r}{\beta}\right)^2\right)\right]$$

$\alpha \approx 4.1$ nm
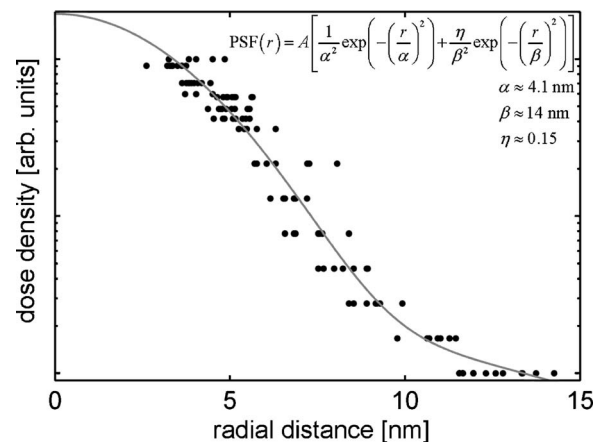$\beta \approx 14$ nm
$\eta \approx 0.15$

FIG. 4. Lithographically estimated point-spread function (PSF) of our focused helium-ion beam for HSQ on silicon. Dose density, which is proportional to the reciprocal of beam dwell time in our dose vector experiment, is plotted on a log scale vs half the measured pillar diameter. For each dose, we measured from scanning-electron micrographs the widths of ten randomly selected pillars in a 50 nm pitch, rectangular pillar array. A double-Gaussian function (the gray curve) was used to fit the data, although a number of functions may be appropriate for the tail of the distribution.

IV. DISCUSSION

The lithographic point-spread function of our helium-ion beam was larger than desired. In particular, the PSF was comparable to that of a good electron-beam-lithography process. What hindered robust sub-10 nm resolution? Possible culprits were the resist, the exposure tool/process, the pattern development process, and metrology.

HSQ may not be capable of sub-4 nm half-pitch, to verify our $\alpha \approx 4.1$ nm result; such half-pitch has not yet been reported in literature to the authors' knowledge. Craver *et al.* found a similar limit for PMMA exposure with 30 keV He atoms;[20] Ocola and Stein found a similar limit for ZEP 520 exposure with an electron beam and cold development.[21] However, since 4.5 nm half-pitch structures have been resolved in HSQ using electron-beam lithography and with less resist residue between features than our 5 nm half-pitch structures,[17] HSQ may not be the primary limiter at this time. One next step would be to use a thinner film of HSQ (≈ 10 nm instead of the ≈ 30 nm used in this study).

Although care was taken to properly focus the helium-ion beam and correct for stigmation, changes in parameters of the microscope during exposure may have caused it to deviate from its sub-nanometer-spot-size specification. For example, as mentioned previously, the gun tip heated up during exposure sessions, which decreased probe current and may have caused aperture misalignment. Other potential sources for beam blurring include mechanical vibration and signal stability in both the microscope and pattern generator electronics. Any of these factors may have established the larger-spread ($\beta \approx 14$ nm) Gaussian as 15% of the measured exposure PSF. Finally, it is possible that optimum focus/stigmation could not be achieved due to sputtering of the focus-target features.

Our development process may be limited in its ability to clear unexposed regions in very densely patterned areas and in its ability to keep high-aspect-ratio (height:width) features from collapsing. The first limitation, self-terminating development, may be due to charge screening at the resist surface;[17] the developer fluid may not be able to extract unexposed HSQ from sub-4 nm half-pitch regions because surface charge may impede developer-ion presence in these regions. The second limitation, collapse of small, high-aspect-ratio features (presumably due to capillary action during drying), may be reduced by supercritical drying.

Our current tool for dimensional metrology is the FE-SEM, which is adequate for the results presented, but since the scanning helium-ion microscope may be capable of patterning with higher resolution than the SEM can image, a higher-resolution metrological tool such as a transmission electron microscope or nanotube-tipped atomic force microscope may be required eventually.

V. SUMMARY AND FUTURE OUTLOOK

We successfully fabricated 20 nm pitch structures with good feature separation and 10 nm pitch structures with poor, but resolvable, feature separation. This resolution is comparable to that of electron-beam lithography. The helium-ion dose required to print features in HSQ on silicon was roughly an order of magnitude smaller than that required with electrons. We also measured the point-spread function for helium-ion exposure of a thin film of HSQ on silicon; the PSF indicates a reduction in the micrometer-range proximity effect typical in electron-beam lithography.

Our technique employed a commercially available helium-ion microscope, pattern generation system, and materials process (HSQ resist on silicon) with a minimal amount of custom equipment and specialized materials/chemicals. Note, however, that we have set only an upper limit on the resolution of helium-ion lithography.

[1]C. A. Volkert and A. M. Minor, MRS Bull. **32**, 389 (2007).

[2]J. Melngailis, Nucl. Instrum. Methods Phys. Res. B, **B80–81**, 1271 (1993).

[3]R. L. Kubena, J. W. Ward, F. P. Stratton, R. J. Joyce, and G. M. Atkinson, J. Vac. Sci. Technol. B, **9**, 3079 (1991).

[4]R. Ramachandra, B. Griffin, and D. Joy, Ultramicroscopy **109**, 748 (2009).

[5]I. Adesida, E. Kratschmer, E. D. Wolf, A. Muray, and M. Isaacson, J. Vac. Sci. Technol. B **3**, 45 (1985).

[6]H. Namatsu, T. Yamaguchi, M. Nagase, K. Yamazaki, and K. Kurihara, Microelectron. Eng., **41–42**, 331 (1998).

[7]R. Livengood, S. Tan, Y. Greenzweig, J. Notte, and S. McVey, J. Vac. Sci. Technol. B (these proceedings).

[8]S. Hirscher, M. Kümmel, A. Wolter, R. Kaesmaier, and A. Jaeschke, Microelectron. Eng. **61–62**, 351 (2002).

[9]J. Melngailis, A. A. Mondelli, I. L. I. Berry, and R. Mohondro, J. Vac. Sci. Technol. B **16**, 927 (1998).

[10]V. Parekh, E. Chunsheng, D. Smith, A. Ruiz, J. C. Wolfe, P. Ruchhoeft, E. Svedberg, S. Khizroev, and D. Litvinov, Nanotechnology **17**, 2079 (2006).

[11]I. Utke, P. Hoffmann, and J. Melngailis, J. Vac. Sci. Technol. B **26**, 1197 (2008).

[12]K. Horiuchi, T. Itakura, and H. Ishikawa, J. Vac. Sci. Technol. B **6**, 241 (1988).

[13]J. A. Van Kan, A. A. Bettiol, and F. Watt, Nano Lett. **6**, 579 (2006).

[14]R. L. Kubena, F. P. Stratton, J. W. Ward, G. M. Atkinson, and R. J. Joyce, J. Vac. Sci. Technol. B **7**, 1798 (1989).

[15]B. W. Ward, J. A. Notte, and N. P. Economou, J. Vac. Sci. Technol. B **24**, 2871 (2006).

[16]J. K. W. Yang and K. K. Berggren, J. Vac. Sci. Technol. B **25**, 2025 (2007).

[17]J. K. W. Yang, B. M. Cord, J. Klingfus, S. W. Nam, K. B. Kim, M. J. Rooks, and K. K. Berggren, J. Vac. Sci. Technol. B (these proceedings).

[18]R. Menon, D. Gil, and H. I. Smith, J. Opt. Soc. Am. A **23**, 567 (2006).

[19]A. E. Grigorescu, M. C. van der Krogt, C. W. Hagen, and P. Kruit, J. Vac. Sci. Technol. B **25**, 1998 (2007).

[20]B. Craver, A. Roy, H. Nounu, and J. C. Wolfe, J. Vac. Sci. Technol. B, **25**, 2192 (2007).

[21]L. E. Ocola and A. Stein, J. Vac. Sci. Technol. B **24**, 3061 (2006).